Chapter 3

Structural Health Monitoring for Composite Materials

Jian Cai, Lei Qiu, Shenfang Yuan, Lihua Shi, PeiPei Liu and Dong Liang

Additional information is available at the end of the chapter

http://dx.doi.org/10.5772/48215

1. Introduction

1.1. Composite materials

A composite material can be defined as a combination of two or more distinct materials at a macroscopic level to attain new properties that can't be achieved by those of individual components acting alone. Different from metallic alloys, each material keeps its own chemical, physical and mechanical properties [1]. Composite materials have reinforcing and matrix phases. The reinforcing phase with higher strength and stiffness is usually fibers, flakes or particles while the matrix phase can be polymers, ceramics or metals. Composite materials are commonly classified into four types, i.e., fibrous composite materials, laminated composite materials, particulate composite materials and the others [2].

Compared with traditional metallic materials, the main advantages of composites are: a) low destiny and high specific strength and stiffness, which are help for weight savings; b) good vibration damping ability, long fatigue life and high wear, creep, corrosion and temperature resistances; b) strong tailor ability in both microstructures and properties make them easily designed to satisfy different application needs; c) since detail accessories can be combined into a single cured assembly, the number of required fasteners and the amount of assembly labor can be significantly reduced [1].

The above advantages make composite materials wildly used in various fields. In aeronautic structures, composite materials are increasingly utilized to decrease weight for payload and radius purposes. The percentages by weight of composites in USA fighters rise from 2% in F-15E to 35.2% in F-35/CV. The overall structure of Eurofighter Typhoon is composed of 40% carbon-fiber composite materials. For commercial aircrafts, the usage percentages of fiber-reinforced composite materials in latest Boeing B787 and newly-designed Airbus A350-XWB reach 50% and 52%, respectively. To meet the performance and fuel efficiency

requirements, the consumption of composites in automobile industry is growing. The blades of wind turbines are normally made of composites to improve electrical energy harvest efficiency [1]. In ships or infrastructures, the composite materials with high corrosion resistance have received wild acceptance. The brake and engine parts working in high temperature are often fabricated from metal or ceramic matrix composites. In addition, the sports and recreation market is also one of the primary consumers of composites [3].

1.2. Problems of composite materials

Despite having the great advantages and applicability, composite materials are not exempt from some problems. As multiphase materials, composites exhibit distinct anisotropic properties. Their material capabilities, largely relating to manufacturing processes, are dispersive. Furthermore, the mechanisms of flaw initiating, spreading over the composite volume and leading to the ultimate failure are very complicated. So far, clearly description for the damage evolution and fracture behavior in composites remains a challenge work. Both the complex mechanical and damage characteristics can also make the optimization design for composites very difficult. Because of lacking enough data cumulation and available standards, the composite design efficiency usually depends on the designer's experiences and the final structures are easily prone to be over-designed [4].

Another important problem for composites is that they are susceptible to impact damages due to the lack of reinforcement in the out-of-plane direction. In a high energy impact, only small total penetration appears in composites. While in the low or medium energy impact, matrix crack will occur and interact, inducing delamination process. Fibre breakage would also happen on the opposite side to the impact [5]. Moreover, damages can be induced in composites by incorrect operations during manufacture and assembly, aging or service condition.

1.3. Requirements of SHM for composite materials

The common damages in composites are fibre breakage, matrix cracking, fibre-matrix debonding and delamination between plies, most of which occur beneath the top surfaces and are barely visible. They can severely degrade the performance of composites and should be identified in time to avoid catastrophic structural failures.

The conventional non-destructive testing (NDT) methods, such as ultrasonic, X-ray, thermography and eddy current methods can be adopted for detecting damages in composites. However, these NDT methods, merely allowing the off-line testing in a local manner with complicated and heavy equipments, are labor-extensive and time-consuming especially for large-scale structures. Meanwhile, disassembling the tested structures may be required to ensure the inspection area accessible, which can increase the maintenance costs [6-7].

Structural health monitoring (SHM), an emerging technique developed from NDT, combines advanced sensor technology with intelligent algorithms to interrogate the

structural 'health' condition [8]. Different from NDT, the real-time and on-line damage detection via in-situ sensors can be achieved in SHM. Now, the needs of SHM for composites have been continuously increased. The potential benefits of SHM include improving reliability and safety, reducing lifecycle costs and helping design of composite materials.

In the following, after the sensors commonly applied in SHM are presented, some typical SHM methods for composites are reviewed. Hereafter arranged are the two SHM examples on composite structures. Summary and conclusions are given at last.

2. Sensors of SHM

In SHM, various sensors are integrated with target structures to obtain different structural information, such as temperature, stress, strain, vibration and so on. The familiar SHM sensors are resistance strain gages, fibre optic sensors, piezoelectric sensors, eddy current sensors, and microelectromechanical systems (MEMS) sensors.

2.1. Resistance strain gages

Resistance strain gage is a traditional strain sensor element. The gage mainly consists of a resistance grid of thin wire or foil, connector and encapsulation layer, as shown in figure 1(a). With the strain-resistance effect, the grid senses the structure's strain as its resistance value, which can be finally converted to the voltage signal with Wheatstone bridge circuit (seen in figure 1(b)). Resistance strain gage, of very small thickness but high sensitivity, can be easily bonded onto the structures and applicable in high temperature or pressure conditions.

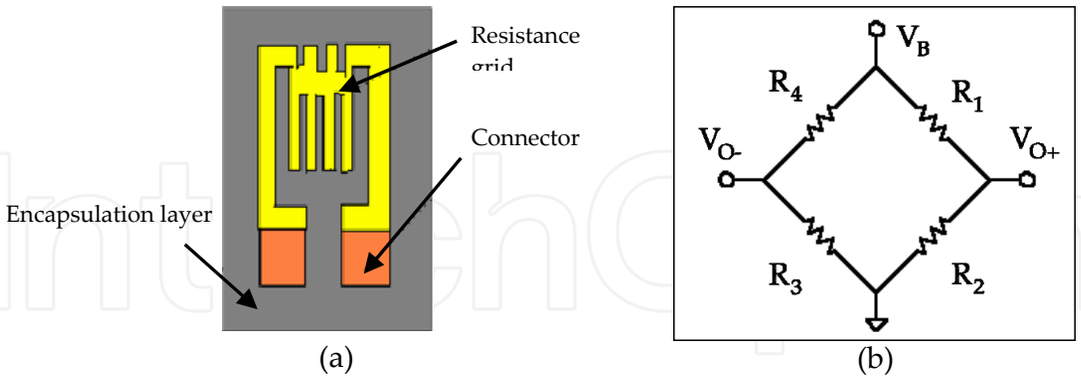

Figure 1. (a) Configuration of a resistance strain gage (b) Wheatstone bridge circuit

2.2. Fibre optic sensors

Fibre optic sensors (FOSs) are competitive candidates for SHM applications because of their unique advantages of light weight, high stability and reliability, long life cycle, low power utilization, EMI immunity, high bandwidth, compatibility with optical date transmission and processing, etc. According to the sensing range, FOSs can be categorized into local,

quasi-distributed and distributed sensors [9]. The most-commonly used local FOSs are interferometric sensors, such as Mach-Zehnder, Michelson and Fabry-Perot FOSs. These sensors can measure strains and deformations at local sites by detecting the phase shifts of relative optical waves.

Fiber Bragg grating (FBG) sensors, with multiplexing capacity, are a kind of typical quasi-distributed FOSs. FBG is formed by inducing a periodic modulation of the refractive index in the core of a single mode optical fiber [10]. When light within a fiber passes through a FBG, constructive interference between the forward and contra-propagating light waves happens and leads to the narrowband back-reflection of light with Bragg wavelength λ_B. Any local changes along with FBG can be manifested as that of λ_B and therefore, from the measurement of the transmitted or reflected spectrum, as shown in figure 2, it is possible to monitor any strain-resulting parameters from temperatures to stress waves [9-11]. The major advantage of the sensor is that an array of wavelength-multiplexed FBGs can be deployed in a single fiber for quasi-distributed measurement. To further increase the number of FBGs, both spatial-division multiplexing and time-division multiplexing can be implemented.

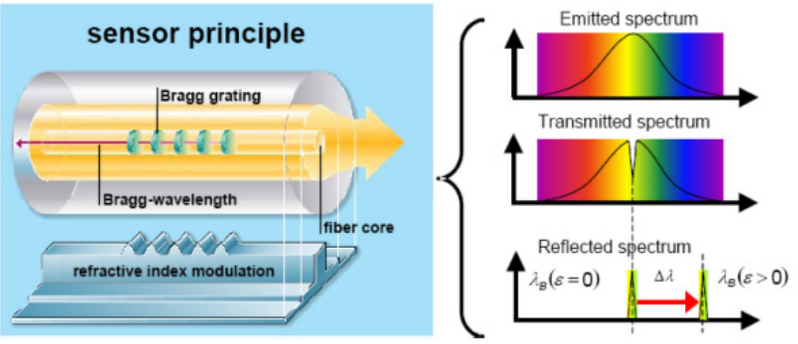

Figure 2. Fiber Bragg grating principle [11]

With all segments of an optical fiber acting as sensors, distributed FOSs can fulfill the real distributed measurement, which is very attractive for SHM of large structures. The sensors are based on the modulation of light intensity in a fiber. The optical time domain reflectometry (OTDR) and Brillouin scattering are the two main distributed sensor methodologies, in which Rayleigh and Fresnel scatterings and Doppler shift in light frequency are used for measuring, respectively [9].

2.3. Piezoelectric sensors

Piezoelectric sensors are frequently used for measuring low or high frequency vibrations, such as Lamb waves or acoustic emission. Compared with conventional acoustic probes, e.g., wedge or comb Lamb wave transducers, piezoelectric sensors are more desired for SHM in view of their weights, sizes and costs. The sensors, made of piezoelectric materials, operate on piezoelectric principles. With direct piezoelectric effect, the sensors in a stress field can generate charge response and vice verse, an external electric field applied to the sensors can result in an induced strain field through inverse piezoelectric effect. Consequently, piezoelectric sensors can be employed both as actuators and sensors [12].

Lead zirconium titanate ceramics (PZT) wafers and polyvinylidene fluoride (PVDF) films are the two common piezoelectric elements, as shown in figure 3. PZT wafers with high piezoelectric constant possess both excellent sensitivities as sensors and strong driving abilities as actuators, whereas the wafers are quite brittle due to ceramic inherent nature. In contrast, PVDF films have the advantages of high flexibility, low mass and cost and high internal damping [13]. However, because of the poor inverse piezoelectric properties and large compliance, PVDF films are usually preferred to be sensors [14]. To overcome the disadvantage of high brittleness of PZT wafers, piezoelectric composites, such as piezoelectric rubbers and piezoelectric paints, have been developed.

Figure 3. PZT and PVDF of various sizes and shapes [14]

2.4. Eddy current sensors

The concept of using eddy currents for damage detection stems from the electromagnetic induction [15], with which the eddy current can be induced to the tested conductive structure and sensed by the identical or different windings of eddy current sensors. The main application of eddy current sensors is crack or corrosion detection for metallic parts even through coatings or layers which may be non-conducting. This makes the sensors useful for such the composite structures as parent metal materials with composite doubler repairs and metal-matrix composites.

Due to the winding configurations, the conventional eddy current sensors with obtrusive size are hard to be integrated. Fortunately, with the development of micro-fabrication technique, the windings can be adhered or directly printed to a conformable substrate. As shown in figure 4, eddy current foil sensors, even in an array style with multiple sensing elements of various shapes, have been produced [16-17]. The new sensors are so thin and flexible that they can be easily surface-mounted or embeded between layers, offering the potential for on-line and continuous monitoring.

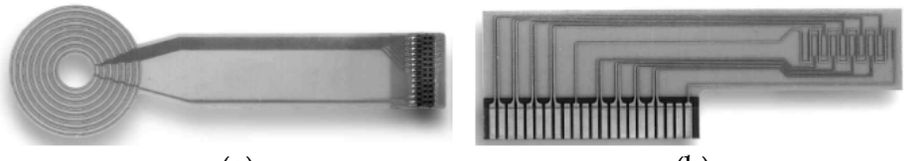

(a) (b)

Figure 4. (a) 4-element rosette eddy current array and (b) 9-element linear eddy current array [18]

2.5. MEMS sensors

With the aid of advanced integrated circuit (IC) fabrication processes, MEMS is developed by co-fabricating microsensors, actuators and control functions in one silicon slice. MEMS is an intelligent system which can sense the circumstances and do some reactions by the microcircuit control [18]. At present, many MEMS sensors, such as MEMS accelerometers and pressure sensors, can be purchased commercially. Due to the extremely small size and large-scale integration degree, the sensors have the remarkable characteristics of light weight, flexibility in design, low power consumption and noise level, short response time, high reliability and economy, etc. To avoid the lengthy cables, the wireless communication capability can be added to the sensors with transmitter chips equipped.

Besides Comparative Vacuum Monitoring (CVM) sensors which will be later introduced together with CVM method, there are other sensors, such as laser scanners and microwave sensors, could be applied in SHM.

With the advances in SHM requirements for both monitoring area and damage quantity, a great number of same or different sensors are arranged to form large sensor arrays to the monitored structure [19], leading to the appearance of various sensor-array layers. Similar to the above eddy current arrays shown in figure 4, the layers are generally made by encapsulating sensor elements with thin and flexible dielectric films in desired configurations. The benefits from the layers are [20]: a) rapidly and consistently arranging a large number of sensors is allowed; b) connecting wires are avoid to reduce EMI; c) the layers can be surface-mounted on existing structures or embeded as extra layers in composites during manufacturing. Besides the PZT-array layer, known as SMART Layer [21], the PZT-FOS hybrid array layer [6] and HELP (Hybrid Electromagnetic Performing) layer [22] have also emerged, as shown in figure 5.

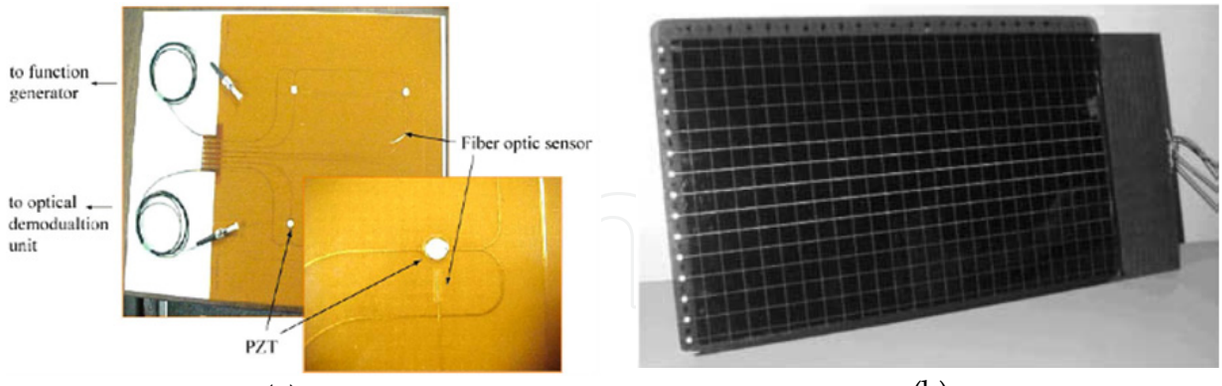

Figure 5. (a) PZT-FOS hybrid array layer [22] (b) HELP layer [23]

3. Typical SHM methods for composite materials

As illustrated in figure 6, SHM can be performed in either passive or active ways depending on whether actuators are used [23]. In passive SHM, various operational parameters, such as loads, stress, acoustic emission and circumstance condition, mainly concerned to infer the

structural states in conjunction with signal and information processing technologies, mechanical modeling analysis or priori-knowledge. Passive SHM only 'listens' to the structures but does not interact with them, as figure 6(a) illustrates. While in active SHM, structures are firstly excited with actuators in prescribed manners and interrogated by analyzing the received structural responses. Though both actuators and sensors are required, as shown in figure 6(b), active SHM can be carried out whenever necessary.

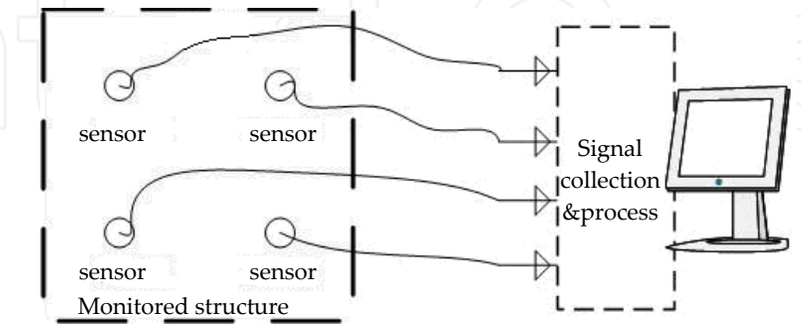

(a) Passive SHM

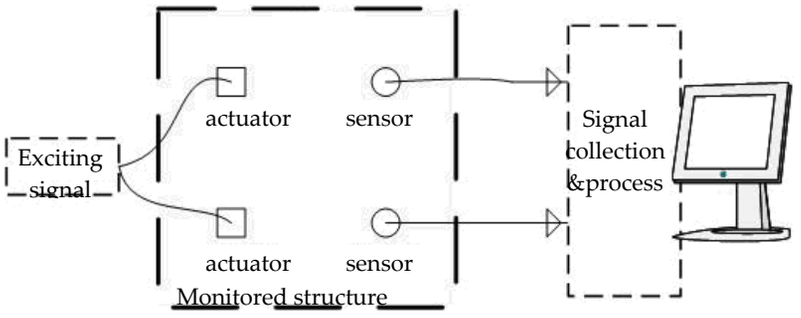

(b) Active SHM

Figure 6. Schemes of passive SHM and active SHM

For composite materials, the common active SHM methods include Lamb wave, Electro-mechanical (E/M) impedance and active vibration-based methods. Acoustic emission, strain-based method and CVM are the typical passive approaches.

3.1. Lamb wave method

Lamb waves, first theoretically predicted by Horace Lamb in 1917, are a kind of guided ultrasonic waves existing in thin-wall structures. Because of the ability of long-distance transmission and high sensitivity to both the surface and the internal defects, Lamb waves are widely used as a promising tool for active SHM.

Lamb waves are usually excited and received by PZT wafers. FOS and PVDF can be also used as the wave sensors. Due to the multi-mode and dispersion characteristics, the propagation of Lamb waves is very complicated. In practical applications, a windowed toneburst is usually selected to generate the fundamental symmetric (S_0) and anti-symmetric (A_0) modes with the excitation frequency below the cut-off frequency of A_1 mode. To

achieve single S_0 or A_0 mode generation, frequency tuning or double-side generation methods can be utilized [24-25].

Since defects in composites can bring about changes of geometric and mechanical boundary conditions, the phenomena of reflecting, scattering and energy attenuation could occur when propagating Lamb waves encounter the defects. Characteristic parameters can be then extracted from Lamb wave signals for damage monitoring.

Damage location is usually based on the time of flight (TOF) of Lamb wave signals. In ellipse location method [26], if the TOF of the damage scattered signal acquired by a transducer pair as well as the propagation velocity is known, an ellipse with the transducer pair at its foci can be determined to indicate the possible flaw locus. In order to identify the exact damage location, more ellipses are required to be constructed with other scattered signals from different transducer pairs and their intersection corresponds to the flaw site. Theoretically, a minimum of three ellipses can unambiguously locate the damage. When mode conversation severely takes place during damage scattering, the TOF of the damage-induced mode signals can be also used to estimate the defect point [27].

Time reversal (TR), based on spatial reciprocity and time invariance of linear wave equations, has been advocated as a baseline-free damage detection method. The presence of damage can induce nonlinearity and break down the reconstruction procedure of TR [28], resulting in divergence between the original and reconstructed waveforms. From the waveform difference, damage index can be then computed, in which original waveform rather than reference signal is involved in.

Damage imaging based on sensor arrays is often performed in Lamb wave monitoring to directly give a display of damage positions and intensities. The familiar imaging methods include delay-and-sum, phased array, and tomography methods.

In delay-and-sum imaging method [29-30], every point of the tested structure is considered as a potential flaw. As shown in figure 7, the traveling time $t_{ij}(x,y)$ of Lamb waves from actuator i at (x_i,y_j) to an imaging point O at (x,y) and then to sensor j at (x_j,y_j) is computed assuming that only one Lamb wave mode exists

$$t_{ij}(x,y) = t_{off} + \sqrt{(x_i - x)^2 + (y_i - y)^2} \Big/ c_i + \sqrt{(x_j - x)^2 + (y_j - y)^2} \Big/ c_j \tag{1}$$

where t_{off} is the reference time, c_i and c_j are the group velocities for the wave mode propagating from i to O and from O and j, respectively.

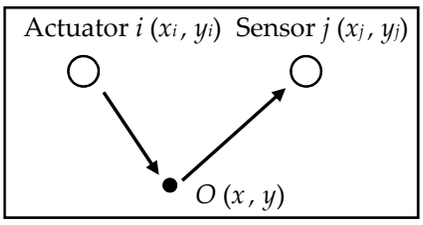

Figure 7. Illustration of delay-and-sum imaging

According to equation (1), the damage scattered signals $s_{ij}(t)$ measured by all transducer pairs can be time-shifted and summarized to get the pixel value at O as

$$E(x,y)=\left[\frac{2}{N(N-1)}\sum_{i=1}^{N}\sum_{j=i+1}^{N}s_{ij}(t_{ij}(x,y))\right]^2 \tag{2}$$

where N is the transducer number.

An image is gained with pixel values at all points calculated. Though delay-and-sum imaging method is very similar to the above ellipse location technique in theory, the special calibration for TOF of every damage scattered signal is not required. Furthermore, those methods [31-32] based on TR focusing are essentially identical to the imaging method.

Phased arrays are generally compact transducer arrays in linear, circular or other patterns. Every array element, commonly PZT wafer, is individually used as actuator and sensor in a round-robin fashion such that a group of sensor signals are collected. Based on the synthetic-beam principles [33], all the signals, supplied with different phase delays, can be combined into one synthetic beamforming signal at one given steering angle, which can be implemented in either time or wavenumber domain [34]. Through the similar processes for all angles, the virtual scanning can be achieved without any physical manipulation of the array. Since constructive interference for the damage scattered signals is actually realized during beamforming, the signal-to-noise (SNR) of diagnostic signals and inspection distance can be largely improved [35]. An image of the scanned area is finally generated by directly mapping all the synthetic signals with the known velocity. Note that phased arrays work in pulse echo mode.

In tomography imaging, an array of transducers should be arranged around the tested area and used for Lamb wave exciting and receiving in pitch-catch mode. A tomographic image can be reconstructed by using wave speed, waveform or amplitude as flaw-relevant features. The standard parallel projection, fan-beam or crosshole schemes are usually adopted in tomography technique [36]. The crosshole scheme with iterative nature and great flexibly is more suited for any geometry and incomplete data set. To increase the sensitivity of tomography with sparse arrays, reconstruction algorithm for probabilistic inspection of defects (RAPID) is introduced [37]. In RAPID, the probabilities of defect occurrence at a point can be estimated from the changing severity of the signal of each transducer pair and its relative position to the pair.

3.2. E/M impedance method

The structural mechanical impendence, defined as the ratio of the applied force to the resulting velocity, can be easily affected by damages, such as cracks, disbonds and delaminations. However, direct measurement for the mechanical impendence is very hard. With PZT transducers, mechanical impendence is indirectly measured as E/M one for damage detection in E/M impedance method [38].

The method utilizes PZT transducers as both actuators and sensors to acquire structural dynamic responses. The electro-mechanical coupling model between the transducer and the structure is shown in figure 8. In the model, the PZT wafer is axially connected to a single degree-of-freedom spring-mass-damper system represented for the structural impendence. Through the mechanical coupling between the transducer and the tested structure and electro-mechanical transduction inside the transducer, the structural impedance gets reflected in the electric one at the transducer terminals as [39-40]

$$Z(\omega)=\left[i\omega a\left(\bar{\varepsilon}_{33}^{T}-\frac{Z_s(\omega)}{Z_s(\omega)+Z_a(\omega)}d_{3x}^2\hat{Y}_{xx}^{E}\right)\right]^{-1} \tag{3}$$

where $Z(\omega)$ is the electric impedance computed as the ratio between the input voltage and the output current of the PZT wafer. $Z_s(\omega)$ and $Z_a(\omega)$ are the structure and PZT wafer mechanical impedances, respectively. a, $\bar{\varepsilon}_{33}^{T}$, d_{3x} and $\hat{Y}_{xx}^{E}$ are the geometry constant, the complex dielectric constant of the PZT wafers at zero stress, the piezoelectric coupling constant and Young's modulus, respectively.

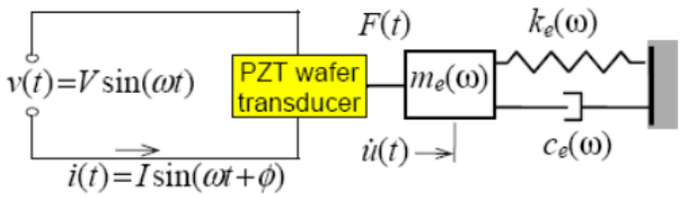

Figure 8. Electro-mechanical coupling model between the PZT transducer and the structure [39]

Equation (3) shows that, as long as the mechanical properties of PZT wafers keep invariable, $Z(\omega)$ is uniquely determined by $Z_s(\omega)$. Thus, the variations of $Z(\omega)$ can be mainly attributed to those of structural integrity. In E/M impedance monitoring, $Z(\omega)$ over a specified bandwidth, i.e., the complex impedance spectrum, is obtained by driving the transducer with sinusoid voltage sweeping and compared with its baseline. Usually, the existence of flaw exhibits as the resonance frequency or amplitude modification in the spectrum. Since the imaginary part of $Z(\omega)$ is temperature-sensitive due to $\bar{\varepsilon}_{33}^{T}$ in equation (3), the real part is more reactive to defects and can be considered for damage assessment. For instance, a damage index is computed as the Euclidean norm of the real portion of the spectrum [39], i.e.,

$$DI=\sqrt{\frac{\sum_{N}\left[R_e(Z_i^1)-R_e(Z_i^0)\right]^2}{\sum_{N}\left[R_e(Z_i^0)\right]^2}} \tag{4}$$

where N is the number of sampling points in the spectrum. Z_i^1 and Z_i^0 are the electric impedances measured in current and health states at frequency sampling point i, respectively.

Note that the impedance measurement is often performed in ultrasonic frequency range. At such high frequencies, the dynamic response is dominated in local modes and the excitation wavelength is small enough to ensure the high sensitivity to incipient local flaws [38-40].

3.3. Active vibration-based method

Active vibration-based method is a classical SHM technique. The basic idea behind the method is that structural dynamic characteristics are functions of the physical properties, such as mass, stiffness and damping [5, 41]. Therefore, damages, arising with physical property changes, can cause detectable differences in vibration responses. The dynamic characteristic parameters commonly used in the method include frequency, mode shape, power spectrum, mode curvature, frequency response function (FRF), mode flexibility matrix, energy transfer rate (ETR), etc.

A typical SHM system based on active vibrations is shown in figure 9.

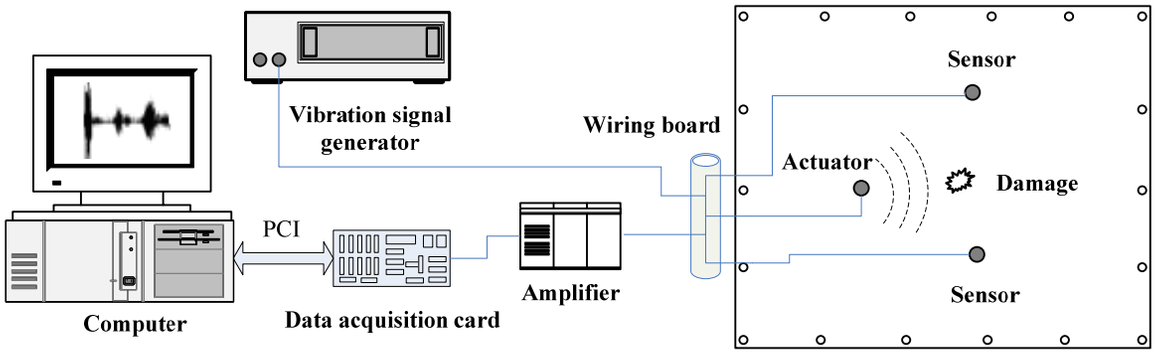

Figure 9. A typical active vibration-based SHM system

The method can be either model based or non-model based. The model-based methods undertake structural model analysis and use model characteristic parameters to identify defects, while non-model based ones permit damage detection relying on the vibration characteristics independent of structural model.

Model-based methods are applied much more in practical SHM applications and can be roughly classified into three groups. One group of the methods, regarded as the forward problems, consists in calibrating model parameters in various known damage cases and defects can be then determined by comparing the measured parameters to the predicted ones. The main challenge of the method is how to obtain the sufficient and accurate characteristic parameters related to all structural circumstances. Particularly for large structures, experimental measurement is unpractical and finite element method (FEM) may a better choice.

In the second group of the methods, criteria or indicators are defined to examine model parameter variations for damage identifying. The ordinary natural frequency criteria are Cawley–Adams criterion and damage location assurance criterion (DLAC). Multiple damage location assurance criterion (MDLAC) is an extension of DLAC to detection multiple flaw sites [42]. Frequency response assurance criterion (FRAC), frequency domain assurance criterion

(FDAC) [43], global shape correlation (GSC) function and global amplitude correlation (GAC) function are the criteria of FRFs [44]. Modal assurance criterion (MAC) can quantify the correlation between measured and analytical mode shapes in a scalar number from zero to unity. The co-ordinate MAC (COMAC) and partial MAC (PMAC) are the developed forms of MAC [5]. The discrepancies of the other model properties, such as mode shape curvature and dynamic flexibility, can be also computed as damage indicators.

The last group of the methods is based on the structural model modification. The discrepancy between the original and modified models can provide the damage information. Mathematically, model modification is a constrained optimization problem based on the structural equations of motion, the nominal model and the measured data [45].

Note that compared with the aforementioned active Lamb wave or E/M impedance methods, the vibration frequencies in the active vibration-based method are generally much lower.

3.4. Acoustic emission method

Acoustic emission (AE) can be defined as the sudden release of localized strain energy in the form of transient elastic wave, due to a distortion or change in the structural integrity of material [46]. Many AEs arise during damage processes within structures. These AEs are referred to as primary ones while the secondary AEs are the others induced from external sources, such as impacts [47].

AE phenomena could appear evidently even when a structure is in microscopic-level damage status, which provides the possibility for defect forecasting and real-time monitoring. Generally, the procedure of AE testing can be summarized as: a) AE waves originate from AE source and propagate to the sensors; b) AE waves are captured by the sensors and converted to electrical signals; c) The AE signals are processed and interpreted to evaluate structural condition. Since only sensors are used to passively detect AE signals, AE method is a passive SHM technique.

From an AE signal, the parameters of AE event, ring-down count, count rate and total count are traditionally extracted to describe the damage mechanisms. The extracting procedures for AE event and ring-down count are illustrated in figures 10 and 11, respectively. As figure 10 shows, providing the envelope picked up from an AE signal with a proper voltage threshold V_1, a square impulse is obtained and related to an AE event. The impulse number over unit time and the accumulative impulse number are respectively defined as event count rate and total event count. If a threshold is directly set to the AE waveform, the ring-down count is gotten by quantitatively recording the resultant ring impulses, as shown in figure 11. Ring-down count per event is the so-called AE rate. The other signal features including amplitude, duration, rise time and energy can be also correlated with the defect characteristics [48]. Additionally, because different damages could result in different frequency contents, the spectrum of the AE signal can be calculated for damage discrimination [49].

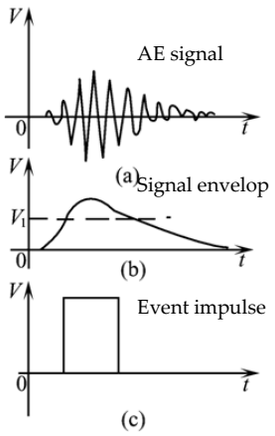

Figure 10. Extracting procedure for AE event

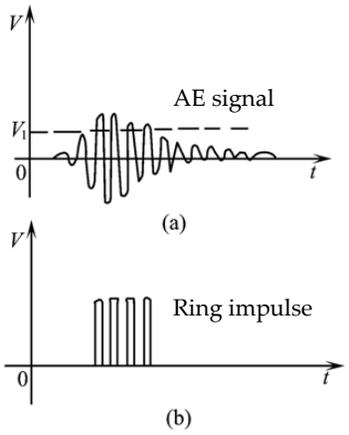

Figure 11. Extracting procedure for ring-down count

Using the time information of AE signals, AE source location can be realized. Taking the triangulation method for example, the location principle is illustrated in figure 12. At least three sensors, P_1, P_2 and P_3, should be used to decide a triangle $\Delta P_1P_2P_3$. As figure 12 shows, supposing AE source S is inside $\Delta P_1P_2P_3$ and the angles between S and the three sensors are θ_1, θ_2 and θ_3, respectively. According to the geometric relationship, a nonlinear equation can be finally derived as

$$\begin{cases} C_{g_1}C_{g_2}\Delta t_{12}\sin(\theta_1+\theta_2)-L_{12}(C_{g_2}\sin\theta_2-C_{g_1}\sin\theta_1)=0 \\ C_{g_2}C_{g_3}\Delta t_{23}\sin(\theta_3+\hat{S}_2-\theta_2)-L_{23}\left(C_{g_3}\sin\theta_3-C_{g_2}\sin(\hat{S}_2-\theta_2)\right)=0 \\ L_{12}\sin\theta_1\sin(\theta_3+\hat{S}_2-\theta_2)-L_{23}\sin\theta_3\sin(\theta_1+\theta_2)=0 \end{cases} \tag{3}$$

where L_{12}, L_{13} and L_{23} are the lengths of three sides of $\Delta P_1P_2P_3$. $\hat{S}_2$ is the internal angle $\angle P_1P_2P_3$. C_{g_1}, C_{g_2} and C_{g_3} are the velocities for the AE waves propagating from S to P_1, P_2 and P_3, respectively. Δt_{12} and Δt_{23} are the arrival time differences between P_1 and P_2, and between P_2 and P_3, respectively.

Note that equation (3) can be also applicable when S is outside $\Delta P_1P_2P_3$. By solving the equation (3), θ_1, θ_2 and θ_3 can be gained to locate S.

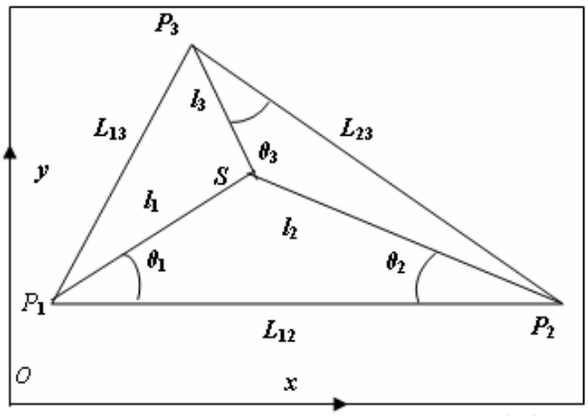

Figure 12. Illustration of triangulation method

For plate-like structures, modal AE (MAE) [50-52] is often presented based on elastic wave theory. In MAE, AE signal is analyzed in terms of different propagating wave modes, among which the basic A_0 and S_0 modes are mostly concerned.

3.5. Strain-based method

Strain-based method is an effective passive SHM method, because the presence of damage in the structure under normal operational loads can alter the local strain distribution due to the changing load path [53]. Besides the resistance strain gages, FOSs are usually applied in the method to measure the distributed strains. Figure 13 gives a typical strain distribution measurement system based on an array of multiplexed FBG sensors.

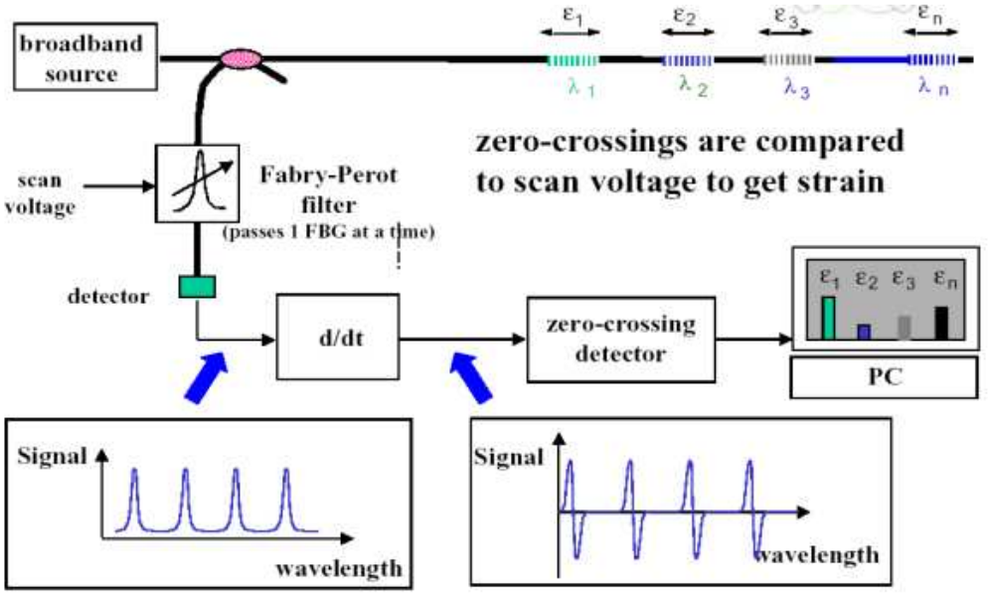

Figure 13. A strain distribution measurement system based on FBG sensors

In practical applications, the strain-based method can be performed in two ways. In one way, the strain distribution of the intact structure is measured as the baseline in advance. Damage can be then detected when the current strain measurement significantly diverges

from the baseline. In the other way, a theoretical model for the structure is established and analyzed to acquire the strain data corresponding to various structural states. Comparing the data to the actually acquired ones directly or with criterions, the structural integrity is evaluated. The key issue lies in this methodology is how to make the model exact enough especially for the complex real-life structure.

3.6. CVM method

CVM method is a very mature technique and is ready for deployment onto operational platforms [54]. CVM has been developed by Structural Monitoring System Ltd. (SMS), with the original patents being granted in 1995. The CVM system has three primary components: a CVM sensor, fluid flow meter and stable low vacuum source [55]. The CVM sensor is directly adhered to the surface of the monitored structure to form a series of long and narrow galleries, which are alternately placed in the low vacuum or atmosphere states, as figure 14 illustrates. With the stable vacuum reference provided by the vacuum source, the air pressure of vacuum galleries is measured by the flow meter. If no flaw presents, the galleries remain sealed and there should be no leaks and pressure changes happening. However, if a flaw develops and breaks the galleries, air will flow along the breakage passage from the atmosphere to the vacuum galleries, increasing the pressure [54, 56]. Furthermore, the rate of pressure rising can be the indication of damage size.

Obviously, the sensitivity of the CVM sensor is determined by the gallery wall thickness. Now, the commercially available sensor can have a sensitivity down to 250μm with an accuracy better than 4% [55]. Since the exposed structural surface becomes one part of the galleries, CVM method is very suitable for surface crack or corrosion detection in metals. Using embedded CVM sensor, the applicability of the method for monitoring crack growth, debonding or delamination in composite structures has been also demonstrated.

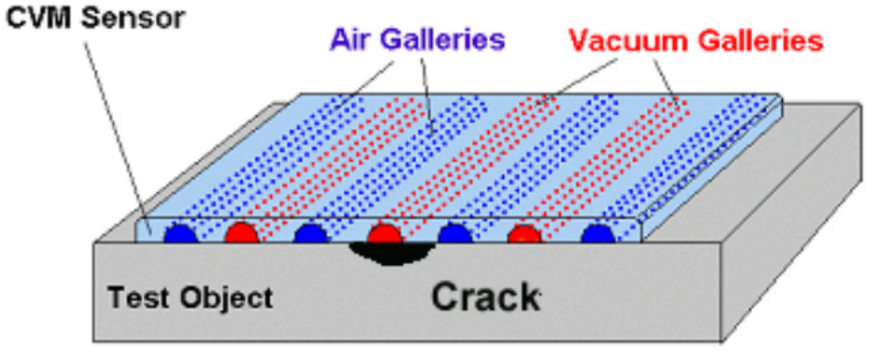

Figure 14. Measuring principle of CVM [61]

All the above methods can be summarized in table 1.

Methods	Used sensors	Monitoring objects					Characteristics
		Strain	Impact	Debonding	Delamination	Crack	
Lamb Wave method	Piezoelectric sensor	D	D	E	E	E	Global monitoring, high sensitivity, on-line & off-line
	FOS	D	D	E	E	E	Global monitoring, requiring PZT actuators, limited by high-frequency modulation
E/M impedance method	Piezoelectric sensor	D	D	E	E	E	Local monitoring, off-line
Active vibration-based method	Piezoelectric sensor & accelerometer	E	D	E	E	E	On-line & off-line, medium and high frequency vibration and acceleration monitoring
	FOS	E	D	E	E	E	On-line & off-line, low frequency (<1kHZ) vibration monitoring
Strain-based method	Resistance strain gauge	E	D	E	E	E	On-line, relying on loads
	FOS	E	D	E	E	E	Distribution measurement, on-line, rely on loads
Acoustic emission	Piezoelectric sensor & AE sensor	D	E	D	E	E	On-line
CVM	CVM sensor	D	D	E	E	E	Local monitoring, mature method

Table 1. Typical SHM methods for composites

4. SHM examples on composite materials

To verify the SHM methods, two examples of Lamb wave imaging and impact location for composite structures are arranged as the representations of active and passive methods, respectively.

4.1. Lamb wave imaging

The tested specimen is a quasi-isotropic epoxy glass-fiber composite plate with the dimension of 600mm×600mm×2mm. Eight PZT wafers P_1~P_8 are mounted on the plate to form a sparse PZT array, as shown in figure 15. The diameter of each PZT is 8mm and its thickness is 0.48 mm. Two identical hexagonal hollow screws, denoted as D_1 and D_2, are bonded on the plate to simulate damages. The positions of PZT wafers and damages are listed in table 2. The overall experimental setup, including Lamb wave detection system, matrix switch, power

amplifier and the specimen, is shown in figure 16. Lamb wave detection system is built based on an industrial computer, in which a LAI200-ISA arbitrary wave generator (up to 50MHz DAC clock, ±5V output scale, 12 bit resolution), a charge amplifier and a PCI-9812 analog input card (10MHz sampling rate, ±5V sampling scale and 12 bit acquisition resolution) are integrated to generate Lamb wave signals, amplify and collect sensor signals. Matrix switch controls the working sequence of all PZT pairs and power amplifier is used to amplify the excitation signal to enlarge the monitoring area in the plate.

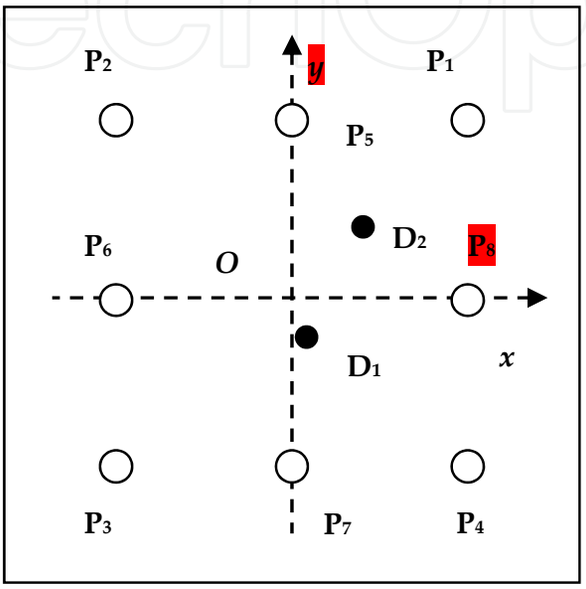

Figure 15. Configuration of the specimen of Lamb wave imaging

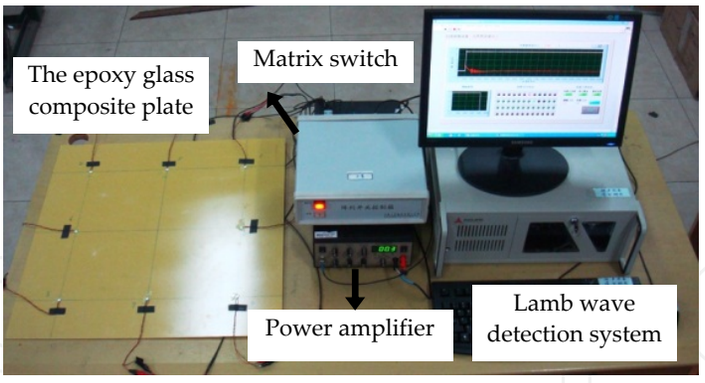

Figure 16. Figure 16 Experiment setup of Lamb wave imaging

	(x, y)/(mm)		(x, y)/(mm)
P_1	(200 , 200)	P_6	(-200 , 0)
P_2	(-200 , 200)	P_7	(0 , -200)
P_3	(-200 , -200)	P_8	(200 , 0)
P_4	(200 , -200)	D_1	(60 , 7 0)
P_5	(0 , 200)	D_2	(10 , -30)

Table 2. The coordinates (x, y) of PZT wafers and damages in the epoxy glass composite plate

As shown in figure 17, a symmetrical modulated 5-cycle sine burst with the central frequency of 50 kHz is adopted to excite diagnostic waves of single A_0 mode into the composite plate. The damage scattered signals can be obtained by subtracting the baseline response of the undamaged plate from the response of the damaged plate under the sin burst excitation. Figure 18 shows the damage scattered signals measured by P_1-P_5 pair. The wavepacket scattered from D_1 can be observed from figure 18(a). When D_1 and D_2 exist, the two damage scattered wavepackts appear in figure 18(b).

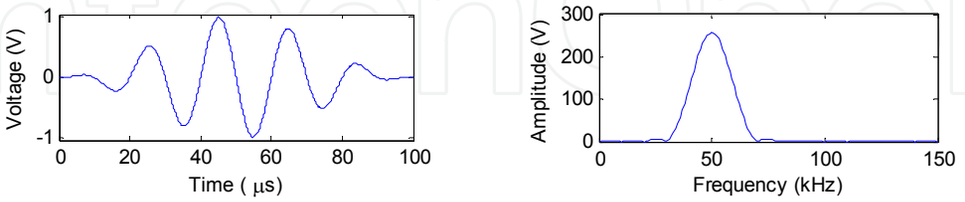

(a) Signal waveform (b) Signal spectrum

Figure 17. Excitation signal

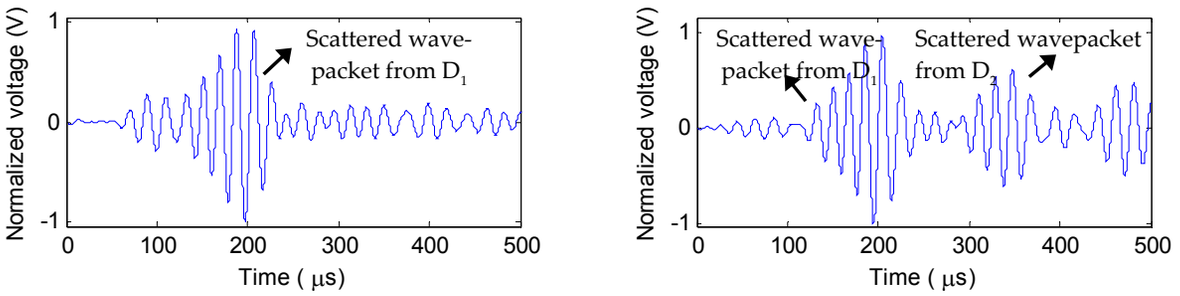

(a) D_1 (b) D_1 and D_2

Figure 18. Damage scattered signals measured by P_1-P_5 pair

After the group velocity of the A_0 mode at 50 kHz is measured as 1331.4m/s in the composite plate, the damage images can be constructed by using the envelopes of the twenty-eight scattered signals acquired by all the PZT pairs in the sparse array based on equation (2). The imaging results are shown in figure 19 where the symbol 'X' denotes the actual damage location. As displayed in figure19 (a) and (b), each flaw point is clearly and accurately represented by a bright focalized spot.

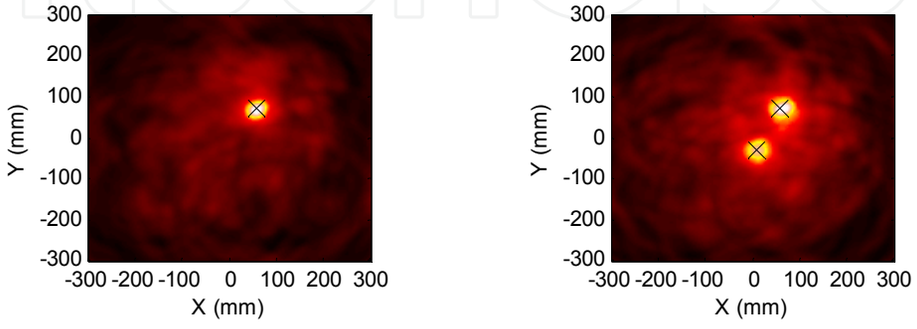

(a) D_1 (b) D_1 and D_2

Figure 19. Imaging results

4.2. Impact location

The experiment system for impact location, mainly composed of an aircraft wing box and an integrated SHM system, is shown in figure 20. The size of the wing box is 1000mm×1800mm×200mm. The top panel is made of carbon fiber composite material and the bottom panel is made of aluminum. The panels are fastened to steel box frame. There are in total six T-shaped stiffeners with a distance of 130mm between each other on the panels. Vertical to the stiffeners there are five rows of bolt holes with a distance of 280mm. The experiment system is built on the top panel of the carbon fiber composite material. An array of smart layers [52] with three PZT wafers is attached on the inner surface of the top panel. Four impacts are produced to the plate using a hammer (seen in figure 20). The detailed positions of the impacts and the used PZT wafers (P_1, P_3, P_4, P_7, P_{16}, P_{19}, P_{20} and P_{22}) are shown in figure 21 and table 3.

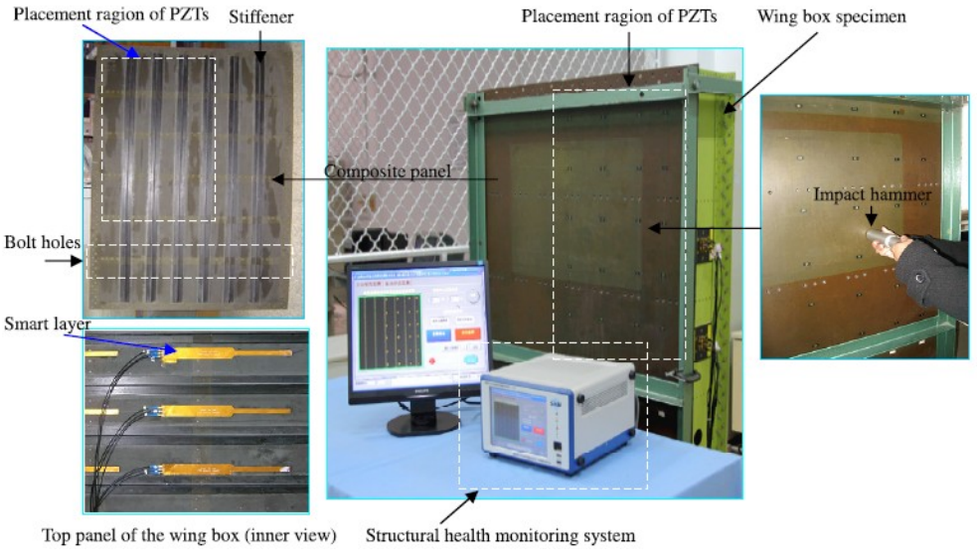

Figure 20. Experiment setup of impact location [52]

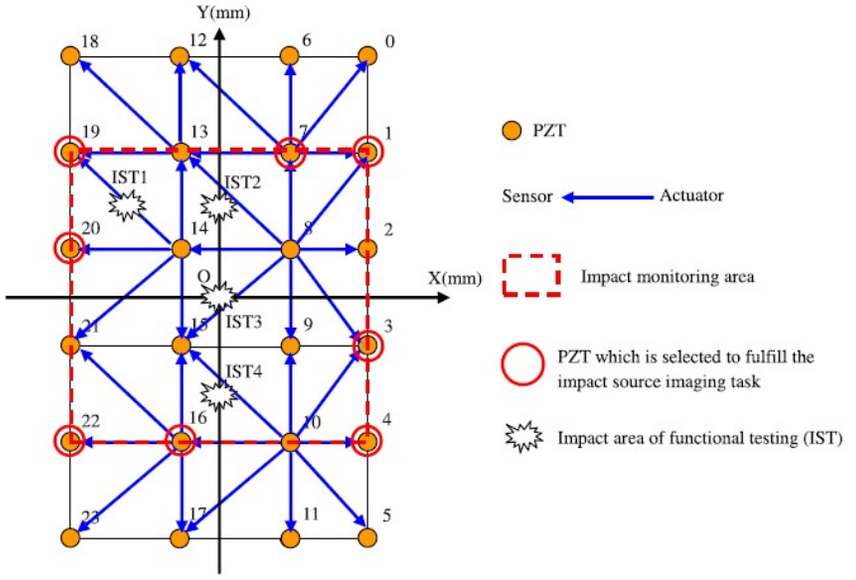

Figure 21. Configuration of the specimen of impact location [52]

	(x, y)/(mm)		(x, y)/(mm)
P_1	(-210 , 225)	P_{20}	(-200 , 75)
P_3	(210 , -75)	P_{22}	(-200 , -225)
P_4	(210 , -225)	IST_1	(-120 , 150)
P_7	(-100 , 225)	IST_2	(0 , 150)
P_{16}	(-50 , -225)	IST_3	(0 , 0)
P_{19}	(-200 , 225)	IST_4	(0 , -150)

Table 3. The coordinates (x, y) of PZT wafers and impacts in the top panel

The impact responses are fed into the integrated SHM system. Figure 22 shows a waterfall plot of normalized responses produced by the impact at IST_1. Here, the narrow-band components with central frequency of 100kHz are extracted from all the responses and their envelopes are then computed for arrival time determination, which can be performed with the complex wavelet transform [57]. After the arrival times are decided by the first peaks in the obtained envelopes, the impact can be located based on equation (3). Note that the anisotropic properties in the composite panel should be considered during impact location. The location result is given in table 4, in which the location error is defined as the spatial interval between the actual and the estimated impact sites.

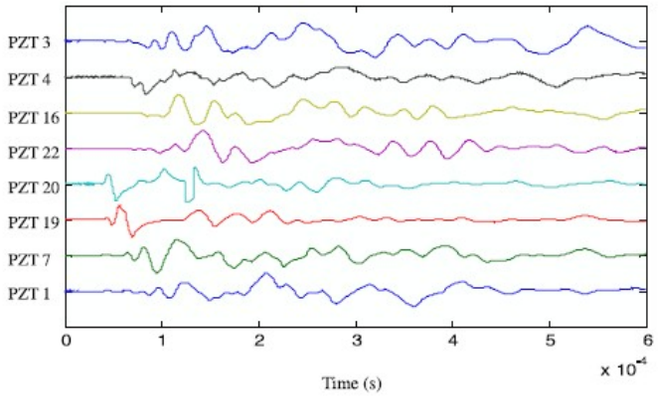

Figure 22. Acquired impact responses [52]

Impact Number	Impact location result		
	Actual site	Estimated site	Location error
IST_1	(-120mm, 150mm)	(-130mm, 125mm)	27mm
IST_2	(0mm, 150mm)	(15mm, 120mm)	16mm
IST_3	(0mm, 0mm)	(0mm, -20mm)	20mm
IST_4	(0mm, -150mm)	(-20mm, -120mm)	36mm

Table 4. Impact location result in the carbon-fiber composite panel

5. Summary and conclusions

SHM for composite materials is briefly described in the chapter. Firstly, an introduction involving advantages, problems and SHM requirements of composites is made. The

common sensors used in SHM as well as typical SHM methods for composite materials are then introduced. Two examples, Lamb wave imaging for a glass-fiber composite plate and impact location in an aircraft composite wing box, are also arranged.

Though much development of SHM has been achieved, a great deal of work is still required for the further practical SHM applications in composite materials.

Author details

Jian Cai, Lei Qiu, Shenfang Yuan, PeiPei Liu and Dong Liang
The Aeronautic Key Lab for Smart Materials and Structures,
Nanjing University of Aeronautics and Astronautics, Nanjing, Jiangsu Province, P.R. China

Lihua Shi
National Key Lab of Electromagnetic Environmental Effect and Electro-optical Engineering, Nanjing, Jiangsu Province, P.R. China

Acknowledgement

This work is supported by EU-FP7 SICA programme (Grant No.FP7-PEOPLE-2010-IRSES-269202), Natural Science Foundation of China (Grant No.50830201).

6. References

[1] Campbell FC. Structural Composite Materials. Ohio: ASM International; 2010.
[2] Jones RM. Mechanics of composite materials (2nd edition). Philadelphia PA: Taylor & Francis; 1999.
[3] Miracle DB, Donaldson SL. Introduction to Composites. In: Miracle DB, Donaldson SL (ed.) ASM Handbook Volume 21: Composites. ASM International; 2001. p3-17
[4] Awad ZK, Aravinthan T, Zhuge Y, et al. A review of optimization techniques used in the design of fibre composite structures for civil engineering applications. Materials and Design 2012; 33(1) 534-544.
[5] Montalvao D, Maia NMM and Ribeiro AMR. A Review of Vibration-based Structural Health Monitoring with Special Emphasis on Composite Materials. The Shock and Vibration Digest 2006; 38(4) 295-324.
[6] Qing XL, Kumar A, Zhang C. A hybrid piezoelectric/fiber optic diagnostic system for structural health monitoring. Smart Materials and Structures 2005; 14(3) S98-S103.
[7] Qing XL, Chan HL, Beard SJ, et al. An Active Diagnostic System for Structural Health Monitoring of Rocket Engines. Journal of intelligent material systems and structures 2006; 17(7): 619-628.
[8] Ihn JB, Chang FK. Pitch-catch Active Sensing Methods in Structural Health Monitoring for Aircraft Structures. Structural Health Monitoring 2008; 7(1): 5-19.
[9] Lia HN, Lia DS and Song GB. Recent applications of fiber optic sensors to health monitoring in civil engineering. Engineering Structures 2004; 26(11): 1647-1657.

[10] Loayssa A. Optical Fiber Sensors for Structural Health Monitoring. In: Mukhopadhyay S. (ed.) New Developments in Sensing Technology for Structural Health Monitoring. Heidelberg: Springer-Verlag; 2011. p335-358.

[11] Speckmann H, Henrich R. Structural health monitoring (SHM) - overview on technologies under development. In: Proceedings of the 16th world conference on NDT (WCNDT). Montreal, Canada, August 30-September 3; 2004.

[12] Lin B, Giurgiutiu V. Modeling and testing of PZT and PVDF piezoelectric wafer active sensors. Smart Materials and Structures 2006; 15(4): 1085-1093.

[13] Boller C. Next generation structural health monitoring and its integration into aircraft design. International Journal of Systems Science 2000; 31(11): 1333-1349.

[14] Raghavan A, Cesnik CES. Review of Guided-wave Structural Health Monitoring. The Shock and Vibration Digest 2007; 39(2): 91-114.

[15] Sodano HA. Development of an Automated Eddy Current Structural Health Monitoring Technique with an Extended Sensing Region for Corrosion Detection. Structural Health Monitoring 2007; 6(2): 111-119.

[16] Zilberstein V, Walrath K, Grundy D, et al. MWM eddy-current arrays for crack initiation and growth monitoring. International Journal of Fatigue 2003; 25(9-11): 1147-1155.

[17] Goldfine N, Zilberstein V, Schlicker D, et al., 2001, Surface Mounted Periodic Field Eddy Current Sensors for Structural Health Monitoring, in Proc. Of SPIE, Advanced Nondestructive Evaluation for Structural and Biological Health Monitoring, ed. T. Kundu, vol. 4335.

[18] Varadan VK, Varadan VV. Microsensors, microelectromechanical systems (MEMS), and electronics for smart structures and systems. Smart Materials and Structures 2000; 9(6): 953-972.

[19] Yuan SF, Liang DK, Shi LH, et al. Recent Progress on Distributed Structural Health Monitoring Research at NUAA. Journal of Intelligent Material Systems and Structures 2008; 19(3): 373-386.

[20] Qing XL, Beard SJ, Kumar A, et al. Advances in the development of built-in diagnostic system for filament wound composite structures. Composites Science and Technology 2006; 66(11-12): 1694-1702.

[21] Lin M, Chang FG. 1998. Design and Fabrication of Built-in Diagnostic for Composite Structures. In: 12th American Society of Composites Technical Conference, Baltimore, USA.

[22] Lemistre MB, Balageas DL. A Hybrid Electromagnetic Acousto-ultrasonic Method for SHM of Carbon/epoxy Structures. Structural Health Monitoring 2003; 2(2): 153-160.

[23] Giurgiutiu V. Structural Health Monitoring with Piezoelectric Wafer Active Sensors. Boston: Elsevier Academic Press; 2008.

[24] Bottai GS, Chrysochoidis NA, Giurgiutiu V, et al. Analytical and experimental evaluation of piezoelectric wafer active sensors performances for Lamb waves based structural health monitoring in composite laminates, 2007, Proceedings of SPIE.

[25] Su Z, Ye L. Selective generation of Lamb wave modes and their propagation characteristics in defective composite laminates. Journal of Materials: Design and Applications 2004; 218(2): 95-110.

[26] Quek ST, Tua PS, Jin J. Comparison of Plain Piezoceramics and Inter-digital Transducer for Crack Detection in Plates. Journal of Intelligent Material Systems and Structures 2007; 18(9): 949-961.
[27] Su ZQ, Ye L, Bu XZ. A damage identification technique for CF/EP composite laminates using distributed piezoelectric transducers. Composite Structures 2002; 57(1-4): 465-471.
[28] Park HW, Sohn H, Law, KH, et al. Time reversal active sensing for health monitoring of a composite plate. Journal of Sound and Vibration 2007; 302(1-2): 50-66.
[29] Michaels JE. Detection, localization and characterization of damage in plates with an in situ array of spatially distributed ultrasonic sensors. Smart Materials and Structures 2008; 17(3): 1-15.
[30] Cai J, Shi LH, Yuan SF, et al. High spatial resolution imaging for structural health monitoring based on virtual time reversal 2011; 20(5): 055018-55028.
[31] Wang HC, Rose JT, Chang FG. A synthetic time-reversal imaging method for structural health monitoring. Smart Materials and Structures 2004; 13(2): 415-423.
[32] Wang Q, Yuan SF. Baseline-free Imaging Method based on New PZT Sensor Arrangements. Journal of Intelligent Material Systems and Structures 2009; 20(14): 1663-1673.
[33] Giurgiutiu V, Bao J. Embedded-ultrasonics Structural Radar for In Situ Structural Health Monitoring of Thin-wall Structures. Structural Health Monitoring 2004; 3(2): 121-140.
[34] Wilcox PD. Omni-directional guided wave transducer arrays for the rapid inspection of large areas of plate structures. IEEE Transactions on Ultrasonics, Ferroelectrics and Frequency Control 2003; 50(6): 699-709.
[35] Yan F, Royer RL, Rose JL. Ultrasonic Guided Wave Imaging Techniques in Structural Health Monitoring. Journal of Intelligent Material Systems and Structures 2010; 21(3): 377-384.
[36] Leonard KR, Malyarenko EV, Hinders MK. Ultrasonic Lamb wave tomography. Inverse Problems 2002; 18(6): 1795-1808.
[37] Zhao XL, Gao HD, Zhang GF, et al. Active health monitoring of an aircraft wing with embedded piezoelectric sensor actuator network. Smart Materials and Structures 2007; 16(4): 1208-1217.
[38] Ayres JW, Lalande F, Chaudhry Z, et al. Qualitative impedance-based health monitoring of civil infrastructures. Smart Materials and Structures 1998; 7(5): 599-605.
[39] Giurgiutiu V, Rogers C A. 1998 Recent advancements in the electro-mechanical (E/M) impedance method for structural health monitoring and NDE Proc. Conf. on Smart Structures and Materials (San Diego, CA) vol 3329 (SPIE) pp 536–47.
[40] Gyuhae P, Sohn H, Farrar CR, et al. Overview of Piezoelectric Impedance-Based Health Monitoring and Path Forward. The Shock and Vibration Digest 2003; 35(6): 451-463.
[41] Farrar CR, Doebling SW, Nix DA. Vibration-based structural damage identification. Philosophical transactions of the Royal Society. Mathematical, physical, and engineering sciences 2001; 359(1778): 131-149.
[42] Messina A, Williams EJ, Contursi T. Structural damage detection by a sensitivity and statistical-based method. Journal of Sound and Vibration 1998; 216(5): 791-808.

[43] Pascual R, Golinval JC, Razeto M. A frequency domain correlation technique for model correlation and updating. International Modal Analysis Conference (IMAC), 15th, Orlando, FL; UNITED STATES; 3-6 Feb. 1997. pp. 587-592. 1997.

[44] Zang C, Friswell MI, Imregun M. Structural Health Monitoring and Damage Assessment Using Measured FRFs from Multiple Sensors, Part I: The Indicator of Correlation Criteria. Key Engineering Materials 2003; 245-246(131): 131-140.

[45] Doebling SW, Farrar CR, Prime MB. Review of Vibration-Based Damage Identification Methods. Shock and Vibration Digest 1998; 30(2): 91-104.

[46] Gostautas RS, Ramirez G, Peterman RJ. Acoustic Emission Monitoring and Analysis of Glass Fiber-Reinforced Composites Bridge Decks. Journal of Bridge Engineering 2005; 10(6): 713-721.

[47] Nair A, Cai CS. Acoustic emission monitoring of bridges: Review and case studies. Engineering Structures 2010; 32(6): 1704-1714.

[48] Huang M, Jiang L, Liaw PK. Using Acoustic Emission in Fatigue and Fracture Materials Research. JOM-e 1998; 50(11): 1-14. http://www.tms.org/pubs/journals/JOM/9811/Huang/Huang-9811.html

[49] Groot PJ, Wijnen PA, Janssen RB. Real-time frequency determination of acoustic emission for different fracture mechanisms in carbon epoxy composites. Composites Science and Technology 1995; 55(4): 405-412.

[50] Morscher GN, Modal acoustic emission of damage accumulation in a woven SiC/SiC composite. Composites Science and Technology 1999; 59(5): 687-697.

[51] Surgeon M, Wevers M. Modal analysis of acoustic emission signals from CFRP laminates. NDT&E International 1999; 32(6): 311-322.

[52] Qiu L, Yuan SF, Zhang XY, et al. A time reversal focusing based impact imaging method and its evaluation on complex composite structures. Smart Materials and Structures 2011; 20(10): 105014.

[53] Silva-Munoz RA, Lopez-Anido RA. Structural health monitoring of marine composite structural joints using embedded fiber Bragg grating strain sensors. Composite Structures 2009; 89(2): 224-234.

[54] Mrad N. State of Development of Advanced Sensory Systems for Structural Health Monitoring Applications. Proceedings of the NATO RTO AVT-144 Workshop on Enhanced Aircraft Platform Availability Through Advanced Maintenance Concepts and Technologies, Vilnius, Lithuania, 3-5 October 2006 (DRDC Atlantic SL-2008-260).

[55] Wishaw M, Barton DP. Comparative Vacuum Monitoring: a New Method of In-Situ Real-Time Crack Detection and Monitoring. In: Proceding of 10th Asia-Pacific Conference On Nondestructive Testing, 2001. Brisbane.

[56] Stehmeier H, Speckmann H. Comparative Vacuum Monitoring (CVM) Monitoring of fatigue cracking in aircraft structures. 2nd European Workshop on Structural Health Monitoring July 7-9, 2004 Amazeum Conference Centre at Deutsches Museum, Munich, Germany.

[57] Jeong H. Analysis of plate wave propagation in anisotropic laminates using a wavelet transform. NDT&E International 2001; 34(3): 185-190.